ORIGINAL PAPER

Improved photocatalytic efficiency of bio-synthesised SnO_2 nanoparticle in dye degradation

Ananthi Udhayakumar[1] · Mary Saral Antoney Raj[1] 🄵

Abstract

The main objective of this study is to examine the photocatalytic activity of SnO_2 nanoparticle synthesised by utilising the leaf extract of *Pithecellobium dulce* as a natural oxidant. One-pot green route procedure was followed by calcination at 300 °C. The green synthesised SnO_2 nanoparticle (GS-SNPs) was characterised by various analytical techniques such as UV–Vis diffuse reflectance Spectroscopy (UV–Vis DRS), X-ray powder diffraction (XRD), Fourier transform infrared spectroscopy and thermogravimetric analysis. The size and surface morphology of the particle was studied by scanning electron microscopy, transmission electron microscopy (TEM) and atomic force microscopy. From the results of XRD study, it was found that the average crystalline size of SnO_2 nanoparticle (GS-SNPs) to be 5–9.5 nm. Furthermore, it was confirmed in the range of 5–10 nm as determined by TEM. The photocatalytic activity was tested with amaranth dye and methyl orange with variable concentration (5.0, 7.5, 10, 12.5 and 15 ppm) for optimisation. The efficiency of dye degradation was found to be concentration dependent, and the degradation results were better for amaranth dye than methyl orange with rate constant value of 6.3×10^{-2} and 3.0×10^{-2} min^{-1}. The optimised characteristics are catalyst dosage as 30 mg for 60 min of exposure which resulted in 90.6% for the dye removed. From the observations, it can be concluded that GS-SNPs could open up the possibility of high value exploitation of green-based nanomaterial as efficient photocatalyst in pharmaceutical and chemical industry with minimum cost and non-hazardous environmental impacts.

Graphical Abstract

Extended author information available on the last page of the article
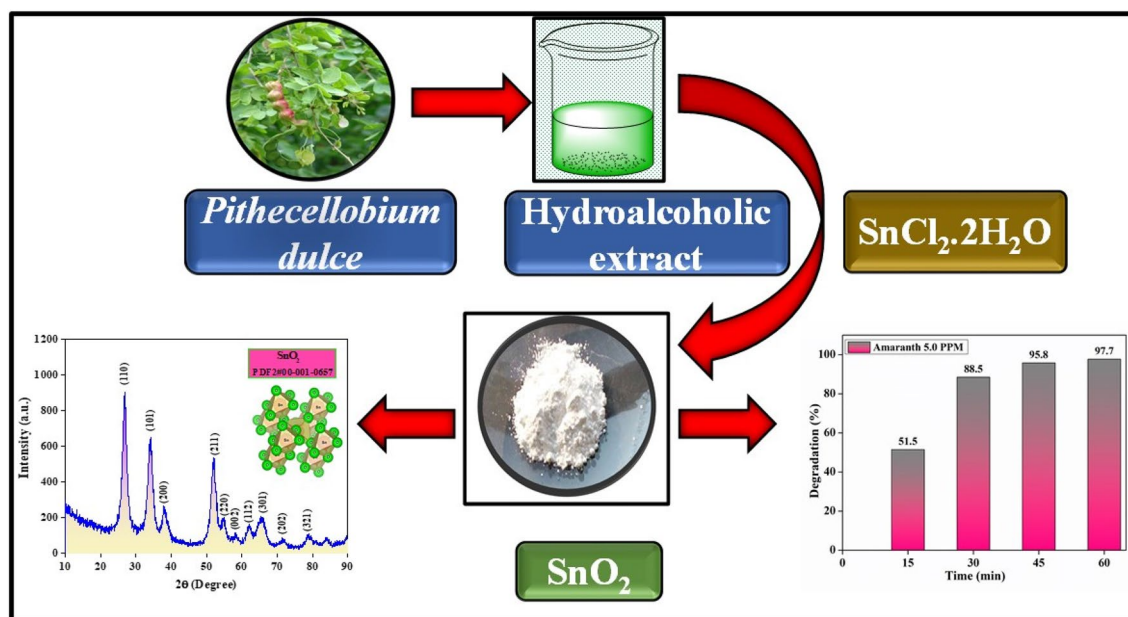
Introduction

Nanoscience and nanotechnology mainly deal with the manipulation of synthesising materials which is constructed by atom and molecule for diverse applications in biological medical fields due to their upturn reactivity as relative to the micro-sized and/or bulk counterparts [1]. Metal oxide nanoparticle has been supreme option to escalate the wide array applications such as nanomedicine, catalysis and photodegradation with respective to the pharmaceutical and chemical industry [2]. According to the metal oxide nanoparticle synthesis, there are several methods that have been followed with the use of (1) organic solvents and/or (2) toxic reducing agents (cetyltrimethylammonium bromide, sodium dodecyl sulphate, NaBH$_4$, ethylene glycol and hydrazine) and also assisted at high temperature treatment, high energy consumption, critical pressure condition in order to get the desirable particle size with no particle agglomeration [3]. Massive part of green nanotechnology ameliorates by renovating the drawbacks which arise in chemical and/or physical method of nanoparticle (NPs) synthesis. Aforementioned trouble of synthesising nanoparticle has been overcome with the aid of green route such as plant parts (roots, leaf, stem, bark, fruit and seed) which were prepared via Soxhlet extraction method, microwave-assisted reaction and reflux methods.

Among the biomass, the plant extracts have potential to elicit the electron-rich phytochemicals (flavonoids, polyphenols etc.) in a good deed of metal oxide nanoparticle synthesis. In the scenario of the nanoparticle synthesis upraising temperature, extensive range of pH and concentration of metal salts were the factors used to validate the metal ion reduction to form a nanoparticle with desirable shape and size. However, choice of plant selection is important to decide the requirement which address oxidant, reductant and or capping agent to form NPs of good size and shape. Synthesis of NPs may be triggered by several compounds such as carbonyl groups, terpenoids, phenolics, flavanones, amines, amides, proteins, pigments, and alkaloids which is present in the plant extracts and microbial cells [4–6].

Pithecellobium dulce, also called Manila tamarind belong to the family Leguminosae possesses tremendous pharmacological applications widely as anticancer, antidiabetic, antiinflammatory and antioxidant property beside *P. dulce* is also reported to have good therapeutic utility [7, 8].

Metal oxide nanoparticle has been used as a best candidate for photocatalytic dye degradation owing to its small size that can attribute easily the binding capacity with the hazardous chemicals produced by industrial waste water systems. In order to find out the cheap and affordable nonconventional technique in waste water treatment green nanotechnology have been engrossed in the synthesis of photocatalytic semiconductor nanomaterials, owing to its huge surface area chemical and physical properties [9–11]. In the literature, it was found that electrolysis, flocculation, precipitation, coagulation, electron beam treatment, activated carbon, oxidation reduction reactions, froth floatation, and photoelectrochemical treatment were used to degrade the organic dye molecules [12–14]. Among various methods on the catalysis (degradation, oxidation, reduction) encapsulation, adsorption of dye will be of great help for better dye removal capacity [15]. Based on the reports, plant derived nanomaterials has been an utmost choice for achieving complete dye degradation of amaranth via one step green process without the use of co-catalyst because of tremendous phytochemical present in the plant extract.

To maintain the eutrophication and aesthetic eco-friendly environment in aquatic life, photocatalytic degradation is reported to be a green technique which is associated with exposure to semiconducting nanomaterial. The material has the capacity of removal of hazardous dyes in the industrial waste water. In this aspect, to overcome the ecological damage caused by recalcitrant toxic dyes which produce relatively stable and carcinogenic degradation product, a lot of attempts have been made in dye degradation with aid of semiconductor nanomaterials as a photocatalyst. Methyl orange and amaranth are water soluble azo dyes and most commonly leads to intestinal cancer on inadvertently entering the body via ingestion. It also produces hazardous degradation products such as aromatic amines which is the main chemical compound responsible for the cancer caused by reductive enzyme which is present in the liver that participates in breakdown of the azo linkage and leads to induce the carcinogenic cell [16, 17].

Moreover, semiconductor material SnO$_2$ NPs has high optical transparency and low electrical resistance in the visible range of the electromagnetic spectrum. These properties make tin oxide suitable for many applications [4, 18, 19]. The large band gap energy of SnO$_2$ of 3.6 eV corresponds to photoactivation in the UV range of the electromagnetic spectrum, makes this material as well as ZnO, used as an ideal photocatalyst for the degradation of a variety of organic pollutants. It is reported that cobalt iron nanoparticle, TiO$_2$, graphene/TiO$_2$-Ag composite under UV light exposure possess amaranth degradation efficiency sequentially 98, 64 and 85% accomplished which it is more than 1 h [20–22]. Photodegradation using the catalyst such as Cu-doped ZnO was studied on visible light exposure which attain 72% of dye degradation efficiency at 180 min [23].

However, to the best of our knowledge, there is no report on the synthesis of SnO_2 nanorod which have a tetragonal crystal system via green route using *P. dulce* leaf. Based on the above consideration in this study, we made an attempt to synthesise and characterise the bio-mediated SnO_2 nanoparticle which is further confirmed by various spectrometric and surface characterisation studies. Thus, the observation made here raise the possibility of (GS-SNPs) as a potential photocatalyst for dye degradation studies.

Experimental section

Bio-mediated SnO$_2$ NPs synthesis

About 20 mg of hydroalcoholic extract was added to 100 mL of distilled water in dropwise under stirring into a beaker containing 20 mmol of stannous chloride solution. The above solution was kept in a water bath for about 3 h. During the period of every 15 min, the reaction mixture was observed under UV to access the completion of the reaction. The precipitate was centrifuged for 30 min and washed several times by using distilled water followed by drying in a hot air oven for about 24 h. The resultant powder was calcinated at 300 °C to get a GS-SNPs.

Preparation of the plant extract

Pithecellobium dulce leaves were collected from Vellore and then washed with distilled water dried at room temperature for two weeks in order to remove the residual moisture. Dried crispy leaves of *P. dulce* were powdered using domestic blender. 70% of the hydroalcoholic extract of *P. dulce* was prepared by using 70 mL of ethanol and remaining water via Soxhlet extraction method. The obtained extract was further concentrated in a rotarvapour and then stored at 5 °C in a refrigerator for further use.

Characterisation

Thus obtained GS-SNPs was characterised by using spectral techniques UV–Visible and FTIR followed by surface characterisation studies such as SEM, BET and TEM [24].

Assessment of photocatalytic degradation

The present study was designed to evaluate the photocatalytic activities of GS-SNPs obtained via green route (*P. dulce*). We explore the effect of the GS-SNPs on photocatalytic degradation of aqueous dye such as methyl orange and amaranth. To monitor the dye degradation of organic azo dyes by using GS-SNPs as a catalyst, experiment was done in a HEBER multi-lamp photoreactor. The study was

initiated by optimising the dye concentration at a specified amount of catalyst (30 mg) which was dispersed into different concentration of dye (5, 7.5, 10, 12.5, 15 ppm) and kept stirred for 30 min in dark to reach the adsorption–desorption equilibrium. During the progress of this reaction, samples were collected in microcuvette between every 15 min until the disappearance of colour of the dye and immediately centrifuged to get a suspension free reaction mixture which is then used for further analysis. To assess the percentage of photocatalytic degradation of dye, the following expression was used as,

$$\text{Degradation efficiency (\%)} = \left(C_0 - C_t/C_0\right) \times 100$$

where C_0 and C_t are the initial concentration of dye after adsorption equilibrium and concentration of dye at time.

Results and discussion

UV-DRS spectroscopy

The synthesised photocatalyst (GS-SNPs) was subjected to UV–Vis DRS spectroscopy to confirm the formation of various types of nanoparticles by measuring plasmon resonance. It was observed that the resultant GS-SNPs showed maximum absorption peak at 370 nm which is the characteristic peak of SnO_2 nanoparticle which usually appear in the absorption spectra range of 300–400 nm. The band gap of the catalyst was found to be 3.4 eV as reported in the literature [25] (Fig. 1).

FTIR spectroscopy

FTIR investigation was performed out on the source extract (HAPD), precursor metal salt solution ($SnCl_2\cdot 2H_2O$) and synthesised resultant nanoparticle GS-SNPs. The FTIR spectra of SnO_2 NPs, $SnCl_2$, and plant extract are shown in Fig. 2a–c which clearly indicates the encapsulation of compound obtained from the presence of bioactive hydroalcoholic leaf extract of *P. dulce* (HAPD) existing on the surface of SnO_2 NPs [26, 27].

X-ray diffraction

XRD patterns of GS-SNPs are shown in Fig. 3 The obtained XRD patterns confirm the tetragonal shape of SnO_2-based on 2θ values of (26.8°, 34.3°, 38.0°, 52.1°, 54.9° and 61.9°) with respective to their plane (hkl) of the unit cell dimension (110), (101), (200), (211), (220), and (112) nearly matched well with PDF2#00-001-0657. Debye–Scherer equation calculated the mean crystal size of produced GS-SNPs,
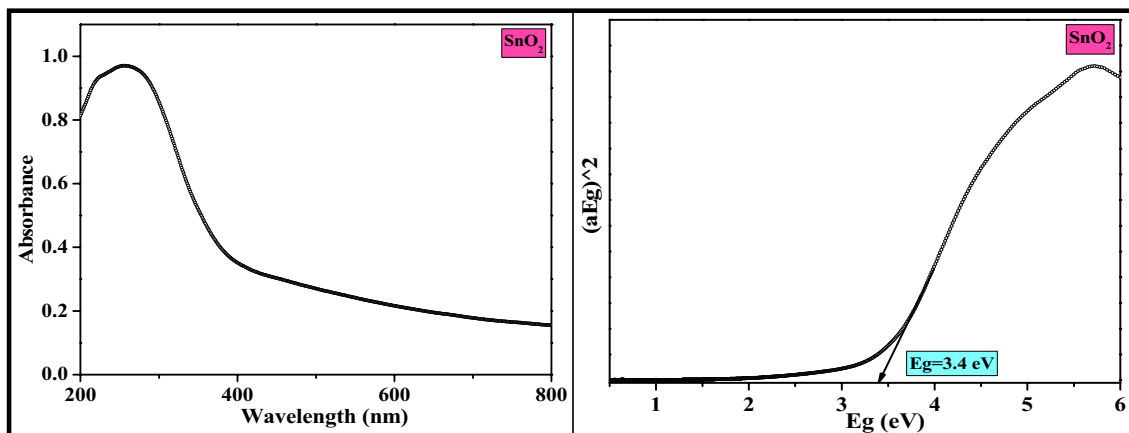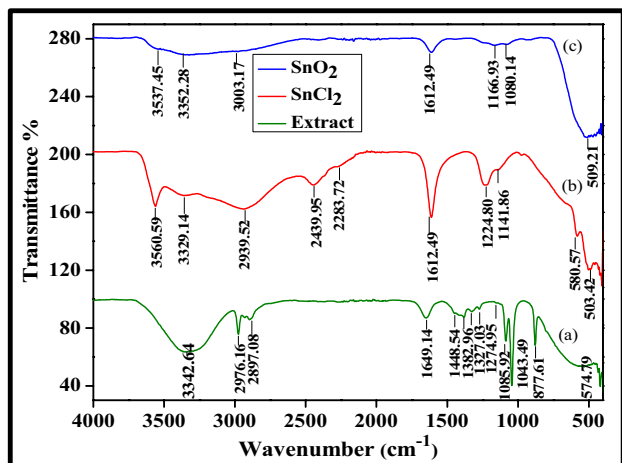
Fig. 1 UV spectrum of GS-SNPs

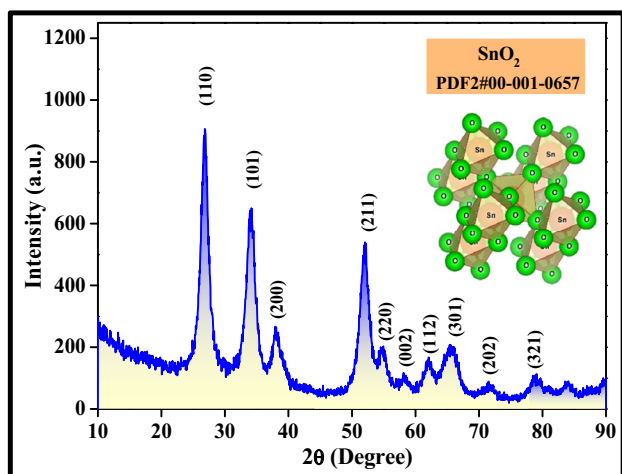**Fig. 2** FTIR graph of SnO$_2$ NPs, SnCl$_2$, and plant extract (HAPD)

Table 1 Average crystalline size of GS-SNPs

Lattice plane (*hkl*)	2θ	β	D (nm)
(1 1 0)	26.8169	1.0584	7.7163
(1 0 1)	34.3406	0.7056	11.7841
(2 0 0)	38.008	0.9408	8.9310
(2 1 1)	52.1289	1.176	7.5201
(2 2 0)	54.9112	0.9408	9.5160
(1 1 2)	61.9649	0.9408	9.8495
	$D_{\text{crystalline}}$		9.2195

$$D = K\lambda/B\text{Cos}\theta$$

where K is the Scherer constant (0.9), λ is the X-ray wavelength of the event (0.154 nm) and β is full width at the half peak limit (FWHM). It strongly suggests that synthesised GS-SNPs forms tetragonal structure with average crystal size was acquired approximately 9.23 nm [4]. From the above consideration, our results nearly match with the small size of crystallinity 9.23 nm with respective unit cell (110), (101) (Table 1).

Thermogravimetric analysis (TGA)

It uncovered the details of weight composition of GS-SNPs. Fig. 4 represents the TGA graph of GS-SNPs. Within the temperature range from 100 to 200 °C, the weight loss of 5.358% may attribute to the loss of low heat of vaporisation materials such as moisture and surface bound water molecules. Also, from 700 to 800 °C stipulate, the decomposition of 15.19% of Sn–O bond that indicate that removal of compound containing oxygen group and carbon frame work belongs to the
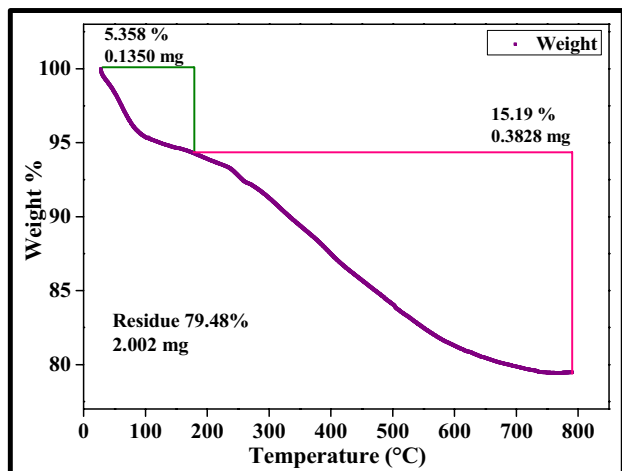

Fig. 3 XRD graph of GS-SNPs

Fig. 4 TGA graph of GS-SNPs

phytochemicals which is present in nanocatalyst may takes place. In other words, decomposition plays vital role in reduction of weight of samples.

Brunauer, Emmett and Teller (BET) surface analysis

BET displayed a relative pressure of 0.40, typical (IV) type and type H3 hysteresis loop were obtained using the present green method. The physical surface area of the GS-SNPs makes them a priority for the dye degradation [11, 28, 29]. It depicts that, in Fig. 5, BET study would be very much helpful to find out the multipoint BET surface 13.407 m^2/g, BJH pore volume 0.130 cc/g, DFT pore size 3.627 nm, respectively.

Scanning electron microscopy (SEM)

The SEM image as shown in Fig. 6a confirmed that, a well-defined nanorod comprises 2.6 μm and 9.01 μm appeared in the magnification power of 15,000× with a bar scale of 2 μm. The EDAX Fig. 6d offers information regarding the amount of element present in the SnO$_2$, further it is revealed that high intensity peak of Sn and low intensity peak due to oxygen were existence of weak signal indicate that reservoir of secondary metabolite (Phenols Flavonoids) in the plant extract which is encapsulated on the surface of GS-SNPs. It is also evident from Fig. 7a–d that the composition in terms of weight percentage of Sn and O as 74.59% and 25.41% and atomic percentage of Sn and O are 28.35% and 71.65%, respectively. This information revealed that Sn and oxygen were homogeneously distributed in GS-SNPs. From Fig. 6 and Fig. 7 it is evident the present study leads to the successful formation of nanorod which have a tetragonal like structure in the range of 2–10 μm well matched with the literature [30].

Atomic force microscopy (AFM)

AFM study clearly confirms Fig. 8 small nano grain agglomeration good agreement with top view of the SEM image. At calcination temperature 300 °C, the surface roughness and crystallite size acquired in the range of 0–100 nm due to the mobility of atom swap their position in adjacent position.

Transmission electron microscopy (TEM)

The morphological and particle size characteristics of GS-SNPs were evaluated by TEM. The morphological HR-TEM image of GS-SNPs photocatalyst shown in Fig. 6b indicates the fringe spacing of 0.318 nm according to the (110) lattice
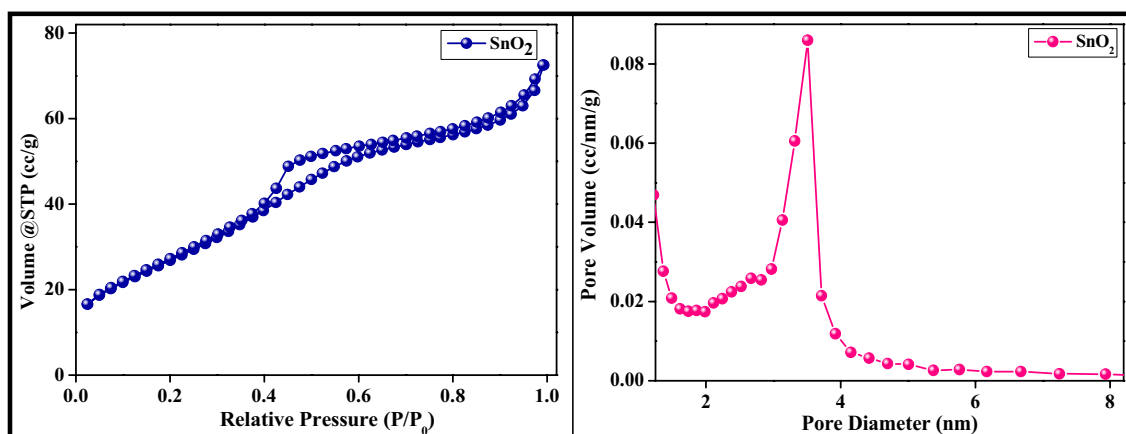

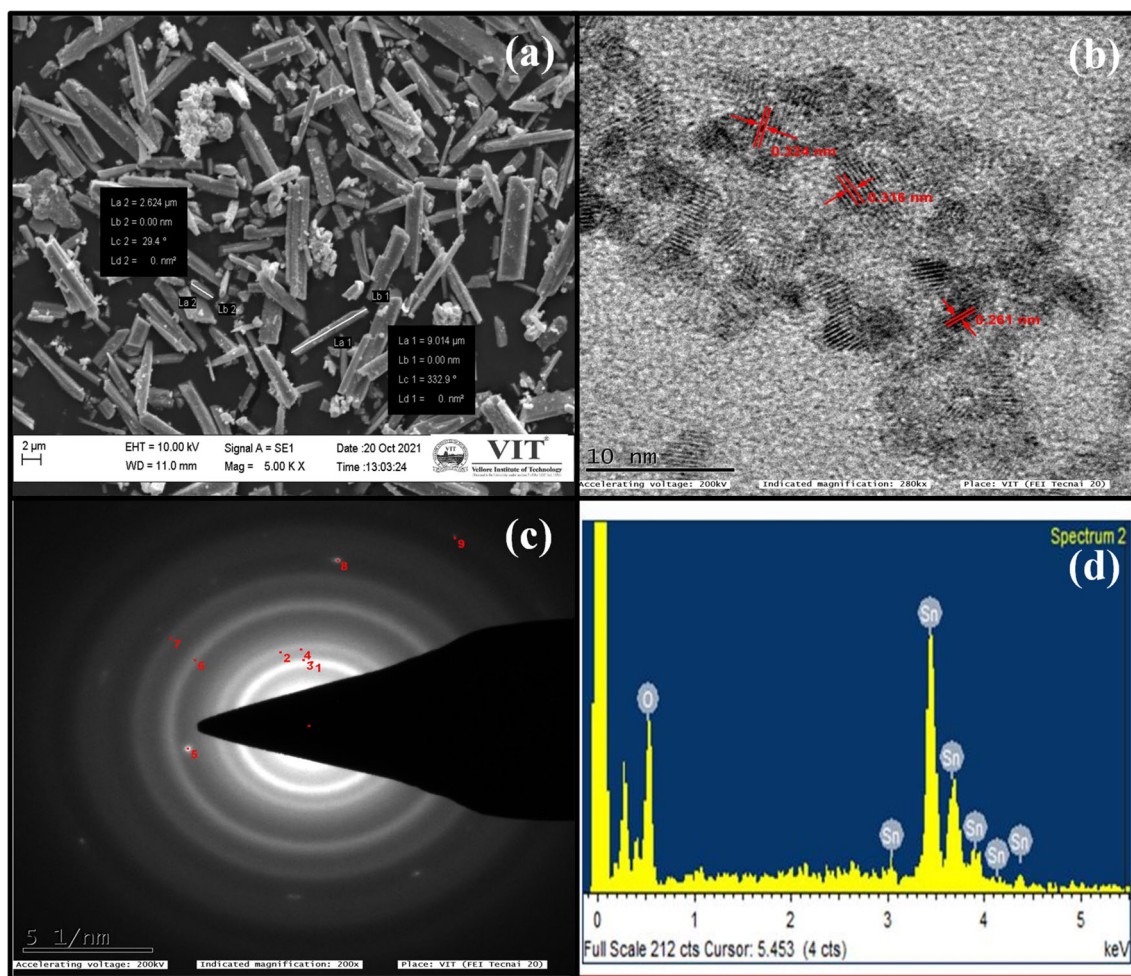**Fig. 5** N$_2$ adsorption–desorption isotherms and pore-size distribution

Fig. 6 **a** SEM, **b-c** TEM image of SnO$_2$ NPs **d** EDAX of GS-SNPs

plane of tetragonal phase of SnO$_2$ with particle size in the range of 11–20 nm. This can be related to the literature [31].

Photocatalytic activity

In Fig. 9, two dyes namely amaranth and methyl orange were selected for evaluating photocatalytic activity of GS-SNPs. Figure 10 depicts the optimisation of dye concentration which was carried using initially 5 ppm concentration of methyl orange and amaranth dye with a fixed dosage GS-SNPs as a catalyst. Amaranth degradation accomplished first-order reaction through linear correlation between ln(C/C$_0$) and time in the form of following equation,

$$-\ln(C/C_0) = kt$$

where C is the concentration of solution at a light irradiation time. C_0 is the concentration solution before the light irradiation, t is the light irradiation time and k is the apparent first-order rate constant.

Adsorption of amaranth dye on GS-SNPs is a primary step to determine the rate of the reaction that accomplish the photodegradation. After 30 min of continuous stirring in the dark with GS-SNPs as a catalyst, 40% of dye removal occurred that indicate the beginning of discoloration. Thus, significant reduction in the initial concentration with absorbance value 0.1767 in situ adsorption takes place on the surface of GS-SNPs. Then, the calculated data have been fitted by plotting $-\ln(C/C_0)$ as a function of time which indicate the amaranth and methyl orange degradation is first-order process with a rate constant value of 6.3×10^{-2} and 3.0×10^{-2} occurred at 60 min and 150 min, respectively. Figure 11 plotted for 5 ppm confirms that the photodegradation of amaranth dye is fast as compared to the methyl orange by means of best linear fit/straight line is obtained. On the other hand, we can say that photocatalytic degradation of amaranth is about two times more efficient than methyl orange. Also it is further observed that there is no significant degradation of methyl orange with 5 ppm whereas amaranth dye responded to the selected catalyst; hence, further studies
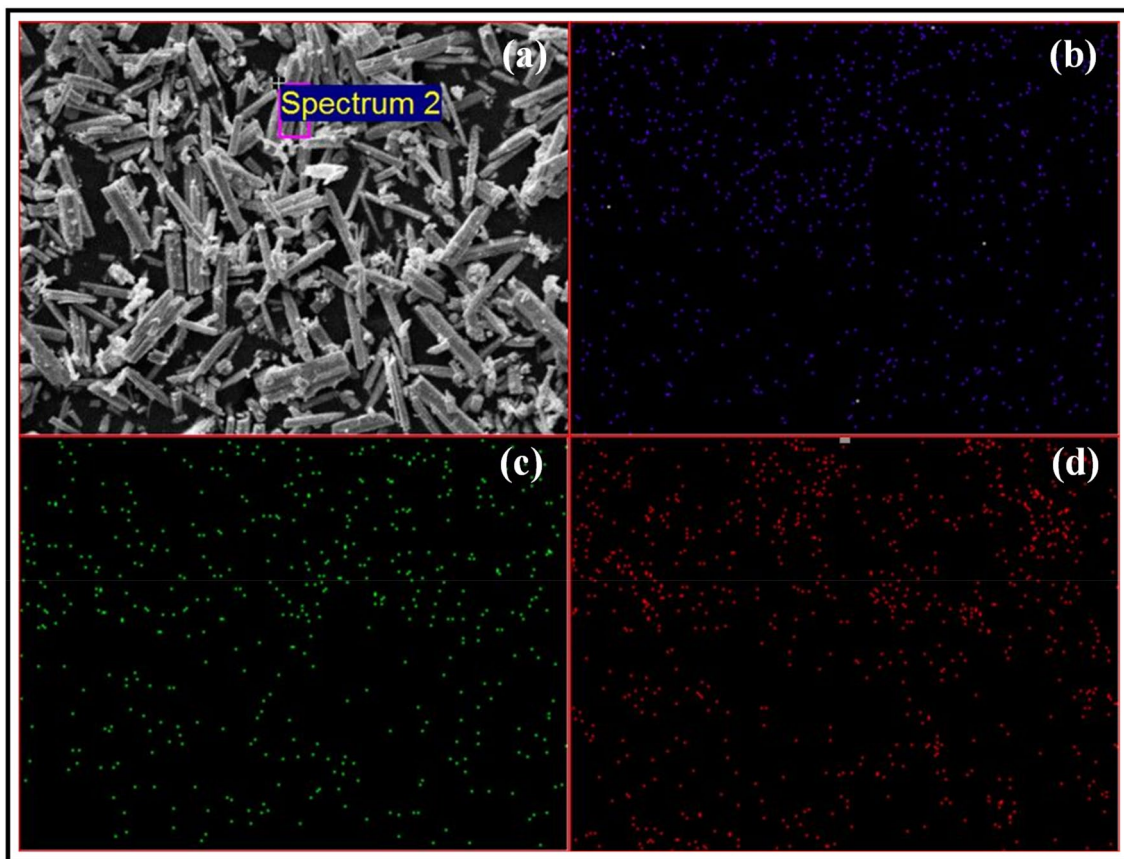
Fig. 7 **a** SEM **b–d** electron image of Sn, O and C present in GS-SNPs

were done with various concentrations, such as 7.5, 10, 12.5, and 15 ppm, of amaranth dye for the assessment of photocatalytic activity of GS-SNPs. The study was repeated using different dosage of catalyst (10, 20, 30, 40 mg) with 10 ppm of amaranth dye. The optimised dosage was subject to study the effect of pH (4, 7, 10). Finally, the reusability of catalyst was evaluated with same concentration of the dye (Fig. 12).

Optimisation of dye concentration

At lower dye concentration, photocatalyst GS-SNPs attains greater potential due to the availability of catalytic surface which allows the penetration of light photons into its active site and as well as dye itself as an internal filter for incident light. Hence, it triggers the formation of OH & O_2^- super oxide radical which could offer the dye degradation. Figure 13 shows the effect of dye concentration, and it was found that when fixed amount of catalyst (30 mg) was dispersed into 5 ppm of Amaranth, 97% dye degradation efficiency occured. The above process can happen in vice versa as dye concentration increase because of hindrance of GS-SNPs catalyst active sites by dye molecule in addition to this smaller number of photons enters the more intense

solution leading to suppress the radical generation eventually reduction in dye degradation efficiency. In other words, as the concentration increases (7.5, 10, 12.5, 15 ppm) it leads to the decrement of dye degradation efficiency (94.3, 90.6, 82.4, 79.9%) at 60 min. Overall, we have taken 10 ppm of the dye with 30 mg of GS-SNPs as the optimum dye concentration for further studies.

Optimisation of catalyst dosage

This study has been made to utilise dye degradation rate which relies on increasing amount of photocatalyst and its active site because of the availability of total surface area for adsorption and light-induced degradation; henceforth, it significantly accelerates the enhanced degradation rate via highest penetration of light with GS-SNPs as a catalyst. Catalyst dosage from 10 to 30 mg gradually enhances the dye removal efficiency, which was about 73.9–90.6% in 60 min. When catalyst load was increased at 40 mg it was observed that 75.1% of the decolourization takes place which may be due to the lower level of penetration of light into a highest catalyst load as compared to the initial quantity of the catalyst. Therefore, it clearly
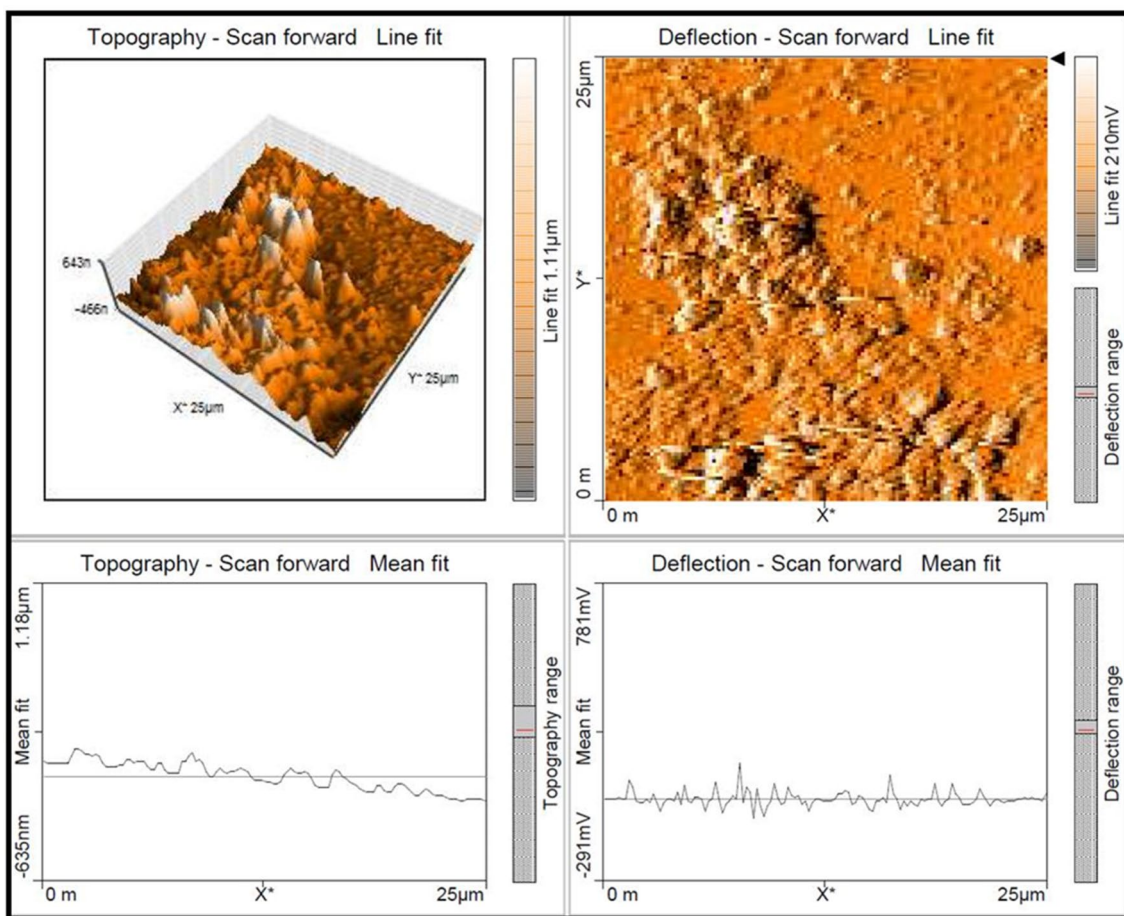
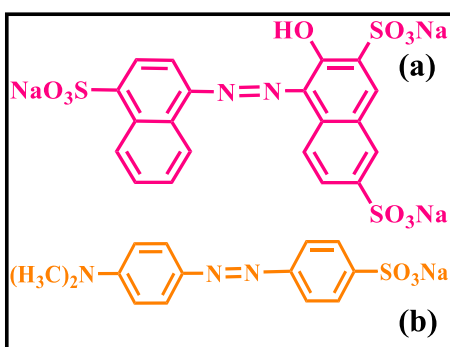**Fig. 8** AFM topographies with 3D structure of GS-SNPs

Fig. 9 Structure of amaranth (**a**), methyl Orange (**b**)

suggests high quantity of catalyst from the optimum amount caused turbidity that leads to decrement of dye removal capacity (Fig. 14).

Optimisation of pH

The impact of pH on this degradation study clearly revealed that the acidic pH; that is, at pH-4, it reaches the efficiency of 90.6% and it is due to the attraction between anionic amaranth dye and GS-SNPs which have the highest dye removal capacity at pH-4 than at pH-10. Generally reactive oxygen species such as OH radical formation promote the reaction between h^+ and OH^- ions causing highest dye degradation efficiency. In contrast, the reason behind the lower level of dye degradation efficiency at basic condition i.e. at pH-10, it is expected that there is an electrostatic repulsion between amaranth dye and catalyst which attribute the restriction of reaction in generating OH radical. Therefore, the present study makes us to conclude that the degradation was efficient at acidic pH-4 as shown in Fig. 15.
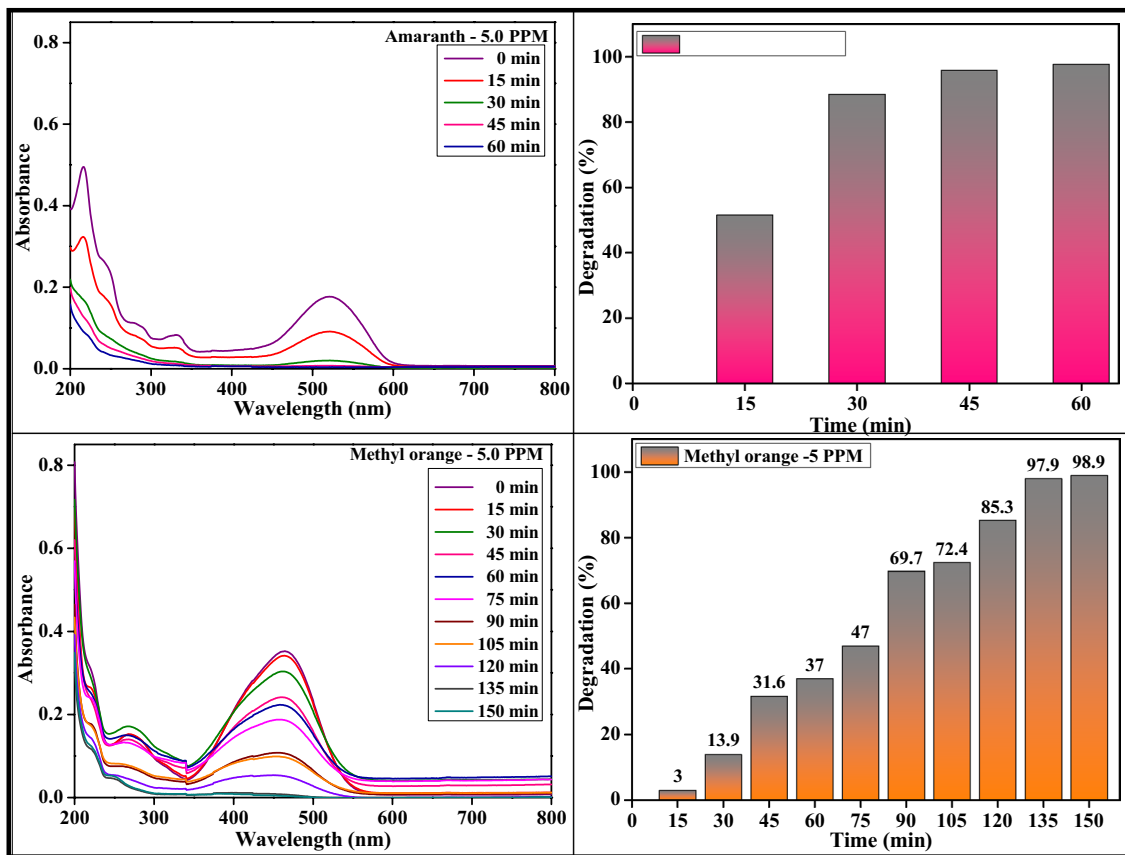
Fig. 10 Comparison of UV absorbance and degradation efficiency of amaranth and methyl orange
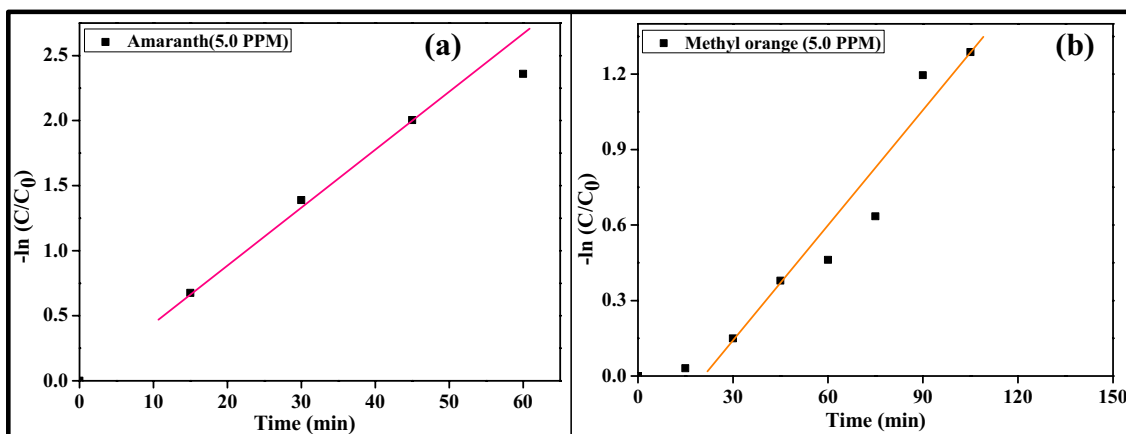

Fig. 11 Kinetic studies of amaranth (**a**), methyl Orange (**b**)

Recyclability

The outcome of this study was promising up to three usages that revealed the crystallinity of the GS-SNPs in cycle-1 is relatively similar to usage of crystallinity of the GS-SNPs in cycle-3. At cycle-4, complete decolourisation occurred in reaction time (125 min) caused by photodissolution of the catalyst might have occurred attribute to its catalytic inactivity (Fig. 16).
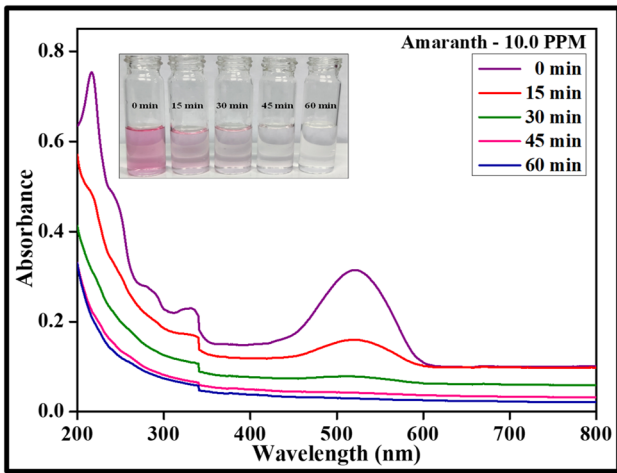
Fig. 12 UV absorbance of optimised dye concentration (10PPM)

Mechanism

Exposure of UV light irradiation into GS-SNPs promotes the decolourisation of organic dyes molecules, and it has been determined by two processes (i.e.) aiming to establish a interaction between valence band and conduction band through the excitation of valence band electrons of the GS-SNPs to conduction band thereby forming of holes in valence band and in the second electrons of the conduction band or holes in the valence band interact with (O_2 or OH adsorbed) surface of the catalyst interaction can happen at O_2 or OH adsorbed active site of catalyst (i.e.) interaction at O_2 or OH adsorbed active site of catalyst which could promote the reactive OH radical involving degradation of dye molecule [16, 18] (Fig. 17).
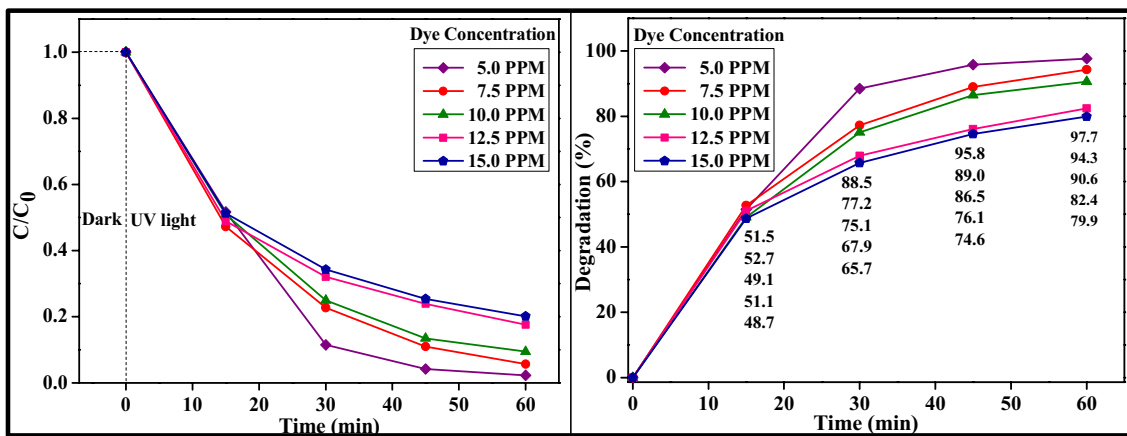

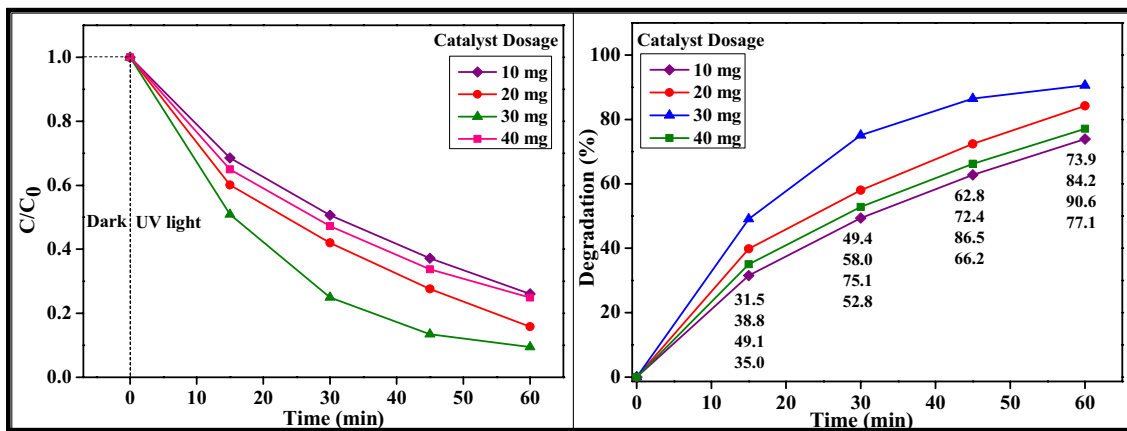**Fig. 13** Degradation efficiency of different dye concentration

Fig. 14 Degradation efficiency of different catalyst dosage
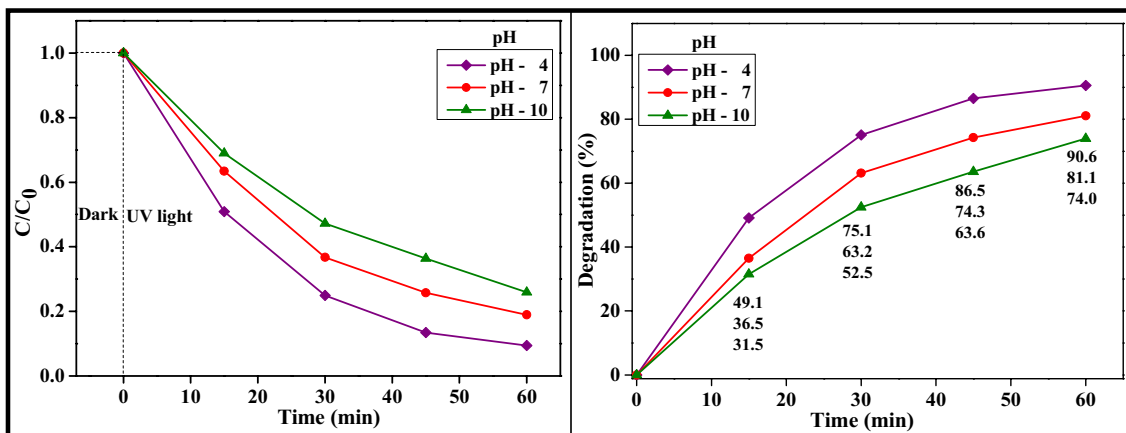
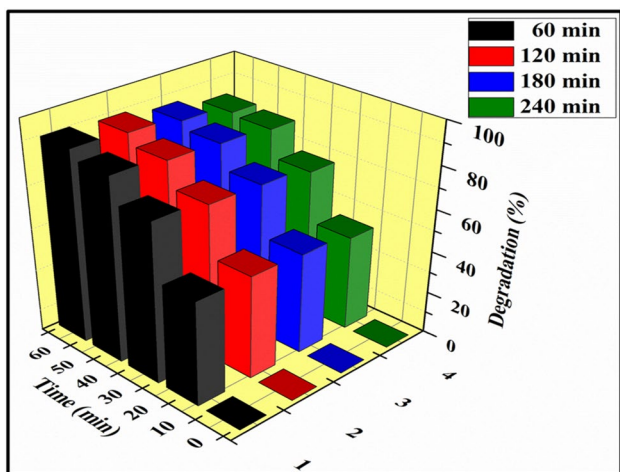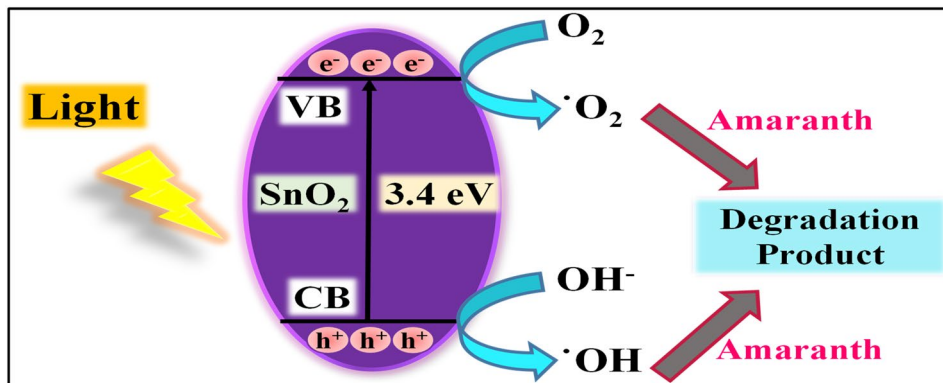**Fig. 15** Degradation efficiency of different pH

Fig. 16 Dye degradation efficiency different runs

Study on dye degradation product

Chromatographic intermediate analysis was attained utilising a HPLC (Waters, model Acquity H/UPLC Class) linked to a PDA e detector using Reliant C185 ™ (4.6 × 150 mm) column and detector set 254, 334, 521 nm corresponding to the maximum absorption wavelength of amaranth. 20 μL of the sample injected which is eluted with aid of the (30:70, v/v) mobile phase (Methanol: ammonium acetate) with a flow rate 0.5 mL/min. HPLC study reveals degradation intermediate product as that of pure amaranth dye with retention time 3.478. The peak at 3.478 is replaced by new peak 3.476 in 15 min time interval at 254 nm. This indicates the degradation process occurs as shown in Fig. 18c. The study indicates that the dye molecule dissociates into intermediates N=N- or C=O with retention time 3.476, 4.621 and 5.462. HPTLC chromatogram showed the variation of Rf occurred between pure Amaranth dye and each 15 min sample. Eventually study concluded that reduced intensity of the peak and its absorbance as well as variation in Rf were provided supplementary substantiation for the degradation of amaranth dye [32]. The data obtained in the present study confirms the possible mechanism for degradation route of amaranth dye and its degradation products with literature results [22, 33] given in Table 2.

Fig. 17 Pictorial representation of mechanism of photocatalytic activity of GS-SNPs
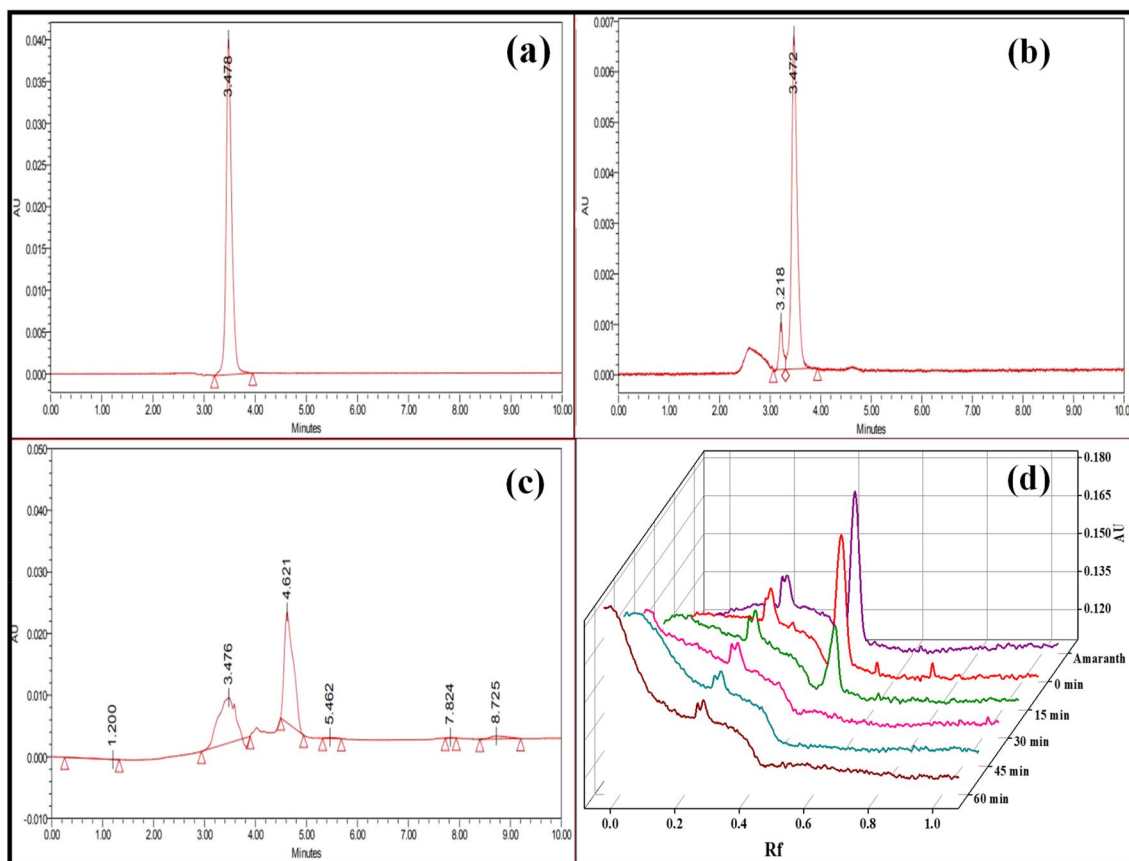
Fig. 18 **a–c** HPLC **d** HPTLC Chromatogram of amaranth dye

Table 2 Literature report on amaranth degradation by using different photocatalyst

Catalyst	Degradation source	Degradation efficiency (%)	Reaction time (min)	References
CoFeNP	UV light	98.85	115	[20]
TiO2 + H₂O₂	UV light	64	100	[21]
Graphene/TiO₂–Ag composite	UV light	85.3–98	120	[22]
Cu-doped ZnO	Visible	72	180	[23]
GS-SNPs	UV light	90.8	60	This work

Conclusion

In summary of the current work, GS-SNPs were prepared with hydroalcoholic leaf extract of *P. dulce*. A systematic study was done on the material with reference to its size, morphology and found that the particle size varied from 11 to 20 nm in tetragonal structure. From the literature, it was reported that the time taken for degradation of amaranth dye was 150 min with maximum efficiency whereas, in our study, it was found that GS-SNPs as a photocatalyst is able to complete the degradation within 60 min. It can be concluded that GS-SNPs is an effective catalyst which degrade the dye in a shorter time. Since there are no chemicals used, the proposed method is green, efficient and safe technology to remove the azo dyes from wastewater.

References

1. Khan S, Shahid S, Sajid M et al (2017) Biogenic synthesis of CuO nanoparticles and their biomedical applications: a current review. Int J Adv Res 5:925–946. https://doi.org/10.21474/IJAR01/4495
2. Rajesh H, Ozkan US (1993) Complete oxidation of ethanol, acetaldehyde and ethanol/methanol mixtures over copper oxide and copper-chromium oxide catalysts. Ind Eng Chem Res 32:1622–1630. https://doi.org/10.1021/ie00020a013
3. Yallappa S, Manjanna J, Sindhe MA et al (2013) Microwave assisted rapid synthesis and biological evaluation of stable copper nanoparticles using *T. arjuna* bark extract. Spectrochim Acta Part A Mol Biomol Spectrosc 110:108–115. https://doi.org/10.1016/j.saa.2013.03.005
4. Haritha E, Roopan SM, Madhavi G et al (2016) Green chemical approach towards the synthesis of SnO_2 NPs in argument with photocatalytic degradation of diazo dye and its kinetic studies. J Photochem Photobiol B Biol 162:441–447. https://doi.org/10.1016/j.jphotobiol.2016.07.010
5. Hussain I, Singh NB, Singh A et al (2016) Green synthesis of nanoparticles and its potential application. Biotechnol Lett 38:545–560. https://doi.org/10.1007/s10529-015-2026-7
6. Mubayi A (2012) Evidence based green synthesis of nanoparticles. Adv Mater Lett 3:519–525. https://doi.org/10.5185/amlett.2012.icnano.353
7. Kulkarni KV, Kaushik C, Kulkarni V, Jamakhandi VR (2018) Medicinal uses of *Pithecellobium dulce* and its health benefits. J Pharmacogn Phytochem 7:700–704
8. Preethi S, Saral AM (2018) Optimization of green methods for extraction of polysaccharides from fruits of *Pithecellobium dulce*. Asian J Chem 30:246–248. https://doi.org/10.14233/ajchem.2018.20759
9. Tahir MB, Nabi G, Khalid NR, Rafique M (2018) Role of europium on WO_3 performance under visible-light for photocatalytic activity. Ceram Int 44:5705–5709. https://doi.org/10.1016/j.ceramint.2017.12.223
10. Tahir MB, Rafique M, Isa Khan M et al (2018) Enhanced photocatalytic hydrogen energy production of g-C_3N_4-WO_3 composites under visible light irradiation. Int J Energy Res 42:4667–4673. https://doi.org/10.1002/er.4208
11. Bilal Tahir M, Sagir M (2019) Carbon nanodots and rare metals (RM = La, Gd, Er) doped tungsten oxide nanostructures for photocatalytic dyes degradation and hydrogen production. Sep Purif Technol 209:94–102. https://doi.org/10.1016/j.seppur.2018.07.029
12. Shanker U, Jassal V, Rani M (2016) Catalytic removal of organic colorants from water using some transition metal oxide nanoparticles synthesized under sunlight. RSC Adv 6:94989–94999. https://doi.org/10.1039/C6RA17555D
13. Nagajyothi PC, Prabhakar Vattikuti SV, Devarayapalli KC et al (2020) Green synthesis: photocatalytic degradation of textile dyes using metal and metal oxide nanoparticles-latest trends and advancements. Crit Rev Environ Sci Technol 50:2617–2723. https://doi.org/10.1080/10643389.2019.1705103
14. Singh J, Kumar V, Kim K-H, Rawat M (2019) Biogenic synthesis of copper oxide nanoparticles using plant extract and its prodigious potential for photocatalytic degradation of dyes. Environ Res 177:108569. https://doi.org/10.1016/j.envres.2019.108569
15. Abdellah AR, Abdelhamid HN, El-Adasy A-BAAM et al (2020) One-pot synthesis of hierarchical porous covalent organic frameworks and two-dimensional nanomaterials for selective removal of anionic dyes. J Environ Chem Eng 8:104054. https://doi.org/10.1016/j.jece.2020.104054
16. Elango G, Roopan SM (2016) Efficacy of SnO_2 nanoparticles toward photocatalytic degradation of methylene blue dye. J Photochem Photobiol B Biol 155:34–38. https://doi.org/10.1016/j.jphotobiol.2015.12.010
17. Mittal A, Malviya A, Kaur D et al (2007) Studies on the adsorption kinetics and isotherms for the removal and recovery of Methyl Orange from wastewaters using waste materials. J Hazard Mater 148:229–240. https://doi.org/10.1016/j.jhazmat.2007.02.028
18. Pan J, Shen H, Mathur S (2012) One-dimensional SnO_2 nanostructures: synthesis and applications. J Nanotechnol 2012:1–12. https://doi.org/10.1155/2012/917320
19. Zhao Q, Ma L, Zhang Q et al (2015) SnO_2-based nanomaterials: synthesis and application in lithium-ion batteries and supercapacitors. J Nanomater 2015:1–15. https://doi.org/10.1155/2015/850147
20. Qurrat-ul-Ain Q-A, Khurshid S, Gul Z et al (2020) Anionic azo dyes removal from water using amine-functionalized cobalt–iron oxide nanoparticles: a comparative time-dependent study and structural optimization towards the removal mechanism. RSC Adv 10:1021–1041. https://doi.org/10.1039/C9RA07686G
21. Gupta VK, Jain R, Mittal A et al (2012) Photo-catalytic degradation of toxic dye amaranth on TiO_2/UV in aqueous suspensions. Mater Sci Eng C 32:12–17. https://doi.org/10.1016/j.msec.2011.08.018
22. Roşu M-C, Socaci C, Floare-Avram V et al (2016) Photocatalytic performance of graphene/TiO_2-Ag composites on amaranth dye degradation. Mater Chem Phys 179:232–241. https://doi.org/10.1016/j.matchemphys.2016.05.035
23. Logamani P, Rajeswari R, Poongodi G et al (2017) Synthesis, characterization and application of Cu doped ZnO nanopowder for the solar photocatalytic degradation of textile dyeing effluent. RJPCBS 8(3S):110
24. Lin P-C, Lin S, Wang PC, Sridhar R (2014) Techniques for physicochemical characterization of nanomaterials. Biotechnol Adv 32:711–726. https://doi.org/10.1016/j.biotechadv.2013.11.006
25. Mayandi J, Marikkannan M, Ragavendran V, Jayabal P (2014) Hydrothermally synthesized Sb and Zn doped SnO_2. Nanoparticles 2:707–710
26. Brightlin Felcia E, Dhinakar Gnanam K (2017) Synthesis and characterisation of SnO_2 nanoparticle by microwave assisted hydrothermal method. IOSR J Appl Phys. e-ISSN: 2278-4861, 98–104
27. Liu H, Wang A, Sun Q et al (2017) Cu nanoparticles/fluorine-doped tin oxide (FTO) nanocomposites for photocatalytic H_2 evolution under visible light irradiation. Catalysts 7:385. https://doi.org/10.3390/catal7120385
28. Abdelhamid HN (2020) Dye encapsulated hierarchical porous zeolitic imidazolate frameworks for carbon dioxide adsorption. J Environ Chem Eng 8:104008. https://doi.org/10.1016/j.jece.2020.104008
29. Chellapandi T, Madhumitha G (2021) Microwave-assisted fabrication of ZnO/MK10 nanocomposite: an efficient photocatalytic and sonophotocatalytic degradation of methylene blue dye. Appl Nanosci 11:1379–1391. https://doi.org/10.1007/s13204-021-01741-7
30. Gnanamoorthy G, Yadav VK, Yadav KK et al (2021) Fabrication of different SnO_2 nanorods for enhanced photocatalytic degradation and antibacterial activity. Environ Sci Pollut Res. https://doi.org/10.1007/s11356-021-13627-w
31. Thamarai Selvi E, Meenakshi Sundar S (2017) Effect of size on structural, optical and magnetic properties of SnO_2 nanoparticles. Mater Res Express 4:075903. https://doi.org/10.1088/2053-1591/aa707d
32. Babu SG, Vinoth R, Neppolian B et al (2015) Diffused sunlight driven highly synergistic pathway for complete mineralization of organic contaminants using reduced graphene oxide supported

photocatalyst. J Hazard Mater 291:83–92. https://doi.org/10.1016/j.jhazmat.2015.02.071

33. Barros WRP, Steter JR, Lanza MRV, Motheo AJ (2014) Degradation of amaranth dye in alkaline medium by ultrasonic cavitation coupled with electrochemical oxidation using a boron-doped diamond anode. Electrochim Acta 143:180–187. https://doi.org/10.1016/j.electacta.2014.07.141

Authors and Affiliations

Ananthi Udhayakumar[1] · Mary Saral Antoney Raj[1] (ID)

✉ Mary Saral Antoney Raj
marysaralvit@gmail.com

[1] Vellore Institute of Technology, VIT University, Vellore, Tamilnadu, India